Science Signaling
AAAS

www.sciencesignaling.org/cgi/content/full/4/176/ra39/DC1

Supplementary Materials for

Antigen Potency and Maximal Efficacy Reveal a Mechanism of Efficient T Cell Activation

Omer Dushek,* Milos Aleksic, Richard J. Wheeler, Hao Zhang, Shaun-Paul Cordoba, Yan-Chun Peng, Ji-Li Chen, Vincenzo Cerundolo, Tao Dong, Daniel Coombs, Philip Anton van der Merwe*

*To whom correspondence should be addressed. E-mail: omer.dushek@path.ox.ac.uk (O.D.); anton.vandermerwe@path.ox.ac.uk (P.A.v.d.M.)

Published 7 June 2011, *Sci. Signal.* **4**, ra39 (2011)
DOI: 10.1126/scisignal.2001430

The PDF file includes:

Methods

Mathematical model

In this section, we first derive the productive hit rate model from the standard serial binding calculations and show how to obtain EC_{50} and E_{max} from the model. The productive hit rate model that we considered contains several simplifications that make the model analytically tractable, but raise the possibility that more realistic models will exhibit different behaviors. We therefore explored variants of the model that included the non-steady-state dynamics of TCR binding and internalization at the end of this section, and found that these models were consistent with our data.

Relation to serial binding calculations

The rate of serial engagements has previously been calculated by noting that the reciprocal of the cycle time for a binding event ($1/k_{on}T$) and an unbinding event ($1/k_{off}$) determines the rate at which a single pMHC molecule serially engages a TCR (*1*):

$$\begin{aligned} & 1/(1/k_{on}T + 1/k_{off}) \\ = \; & k_{off}k_{on}T/(k_{off} + k_{on}T) \\ = \; & k_{off}C/P_T \end{aligned}$$

where T is the concentration of free TCR, C is the concentration of the TCR-pMHC complex, and P is the concentration of free pMHC. As in the main text, a subscripted T indicates total concentrations. We obtained the last line by using the steady-state relation ($k_{on}TP = k_{off}C$) and the conservation of pMHC ($P_T = P + C$). Note that this is the rate of serial binding from a single pMHC, and if we assume there that the approximate numbers of pMHCs at the contact interface are given by P_TA (where A is the area of the interface), then the overall rate of TCR binding is simply: $k_{off}CA$. Finally, we multiplied the rate of serial TCR binding events by the probability that any given event produces productive intracellular signaling and by the total time that the T cell interacts with the pMHC (t), to obtain an estimate for the total number of productive TCR hits:

$$R = k_{off}CAf(k_{off})t$$

where $f(k_{off})$ is a decreasing function of k_{off} between 1 and 0 that determines the probability of a productive signal. This equation is derived more directly in the main text.

Determination of EC_{50} and E_{max}

We first determined EC_{50} and E_{max} from the affinity model dose-response. To determine E_{max}, we calculated the number of occupied TCRs when $P_T \gg K_D$, T_T. This can be calculated in several ways, and the simplest is to simply take the following limit:

$$
\begin{aligned}
\mathrm{E_{max}} &= \lim_{P_\mathrm{T}\to\infty} CA \\
&= \lim_{P_\mathrm{T}\to\infty} \frac{1}{2}\left(P_\mathrm{T}+T_\mathrm{T}+K_\mathrm{D}-\sqrt{(P_\mathrm{T}+T_\mathrm{T}+K_\mathrm{D})^2-4P_\mathrm{T}T_\mathrm{T}}\right)A \\
&= \lim_{P_\mathrm{T}\to\infty} \frac{2P_\mathrm{T}T_\mathrm{T}A}{\left(P_\mathrm{T}+T_\mathrm{T}+K_\mathrm{D}+\sqrt{(P_\mathrm{T}+T_\mathrm{T}+K_\mathrm{D})^2-4P_\mathrm{T}T_\mathrm{T}}\right)} \\
&= \lim_{P_\mathrm{T}\to\infty} \frac{2T_\mathrm{T}A}{\left(1+T_\mathrm{T}/P_\mathrm{T}+K_\mathrm{D}/P_\mathrm{T}+\sqrt{(1+T_\mathrm{T}/P_\mathrm{T}+K_\mathrm{D}/P_\mathrm{T})^2-4T_\mathrm{T}/P_\mathrm{T}}\right)} \\
&= T_\mathrm{T}A
\end{aligned}
\qquad (1)
$$

We now see that $E_{max} = T_TA$ for the affinity model. To determine the concentration of pMHC that produces a half-maximal response (that is, antigen potency, EC_{50}) we solved for P_T in the expression $T_TA/2 = CA$ and found, after some algebra, that $EC_{50} = K_D + T_T/2$.

The determination of E_{max} and EC_{50} for the productive hit rate model is simple, because the dependency on P_T in this model is identical to that of the affinity model. For example, to determine E_{max} in this model we take the following limit:

$$
\begin{aligned}
\mathrm{E_{max}} &= \lim_{P_\mathrm{T}\to\infty} k_\mathrm{off}CAf(k_\mathrm{off})t \\
&= k_\mathrm{off}f(k_\mathrm{off})t \lim_{P_\mathrm{T}\to\infty} CA
\end{aligned}
$$

which is identical to the affinity model. Therefore, in this model we found that $E_{max} = k_{off}T_TAf(k_{off})t$. Similarly, to determine EC_{50}, we solved for P_T in the expression $(k_{off}T_TAf(k_{off})t)/2 = k_{off}CAf(k_{off})t$ and found that $EC_{50} = K_D + T_T/2$.

Validity of the steady-state assumption

For simplicity, we assumed that the interactions between the TCR and pMHC at the contact interface were at steady state. This assumption enabled us to formulate a mathematical model that was analytically tractable, could explain the published data, and could make predictions, which we confirmed experimentally. However, experiments have revealed complicated dynamics, including the transport of TCR to the contact interface, the clustering of TCR at the interface, the transport of TCR clusters within the interface, and the internalization (and recycling) of TCR at the center of the interface (*2*, *3*). There have been efforts to extend the basic productive hit rate model to include these dynamics (*4*, *5*) and other observations [for example, feedbacks in intracellular signaling (*6*, *7*)]. We have not explored these effects because the productive hit rate model, although an approximate model because it is formulated at steady-state and does not include these additional effects, is sufficient to explain our data. The inclusion of these effects would constitute an "over-fitting" of our data, and we have followed the principle of Occam's Razor in our mathematical analysis. We did explore two additional formulations of the productive hit rate model, one of which was a non–steady state model, and found that they were consistent with our basic model (see below).

Alternative productive hit rate models

We assumed that the T cell response is proportional to the productive hit rate. In this model, it is implicitly assumed that each TCR produces only a single productive signal (or a single "ping") upon binding to the pMHC. It is for this reason that an optimal k_{off} emerges, which is independent of the concentration of pMHC. The results from the affinity model (row 1) and the productive hit rate model (row 2) are summarized in fig. S1. In what follows, we examine two alternative formulations of the productive hit rate model.

We can modify the productive hit rate model so that bound TCR continues to signal. In this model, we assume that the total signal from each TCR is proportional to the duration of binding and therefore the signaling rate (R) is given by:

$$\begin{aligned} \hat{R} &= R \times (1/k_{\text{off}}) \\ &= CAf(k_{\text{off}})t \end{aligned}$$

The prediction for EC_{50} was unchanged, but E_{max} no longer exhibited a maximum [$E_{max} = T_T A f(k_{off})t$]. We note that in this model, we never observed an optimal k_{off}. No additional parameters were introduced in this model. The results from this model are summarized in fig. S1 (row 3).

We also considered the effects of TCR internalization in an ordinary-differential-equation (ODE) model, which was adapted from Coombs *et al*. (*4*) (see fig. S2). The system of ODEs governing these dynamics are:

$$\begin{aligned} \partial P/\partial t &= -k_{\text{on}}PT - k_{\text{on}}PT^* + k_{\text{off}}\sum_{i=0}^{N} C_i \\ \partial T/\partial t &= -k_{\text{on}}PT + k_{\text{off}}\sum_{i=0}^{N-1} C_i + \mu T^* + \beta \\ \partial T^*/\partial t &= -k_{\text{on}}PT^* + k_{\text{off}}C_N - (\mu + \lambda_T)T^* \\ \partial C_0/\partial t &= k_{\text{on}}PT - (k_{\text{off}} + k_{\text{p}})C_0 \\ \partial C_i/\partial t &= k_{\text{p}}C_{i-1} - (k_{\text{off}} + k_{\text{p}})C_i \\ \partial C_N/\partial t &= k_{\text{p}}C_{N-1} - (k_{\text{off}} + \lambda_C)C_N + k_{\text{on}}PT^* \end{aligned}$$

where P, T, and C are the concentrations of free pMHC, free TCR, and the TCR-pMHC complex, respectively. The intermediate signaling complexes are denoted by a subscript *i* (C_i) and the productive signaling state is C_N. In this model, C_N is subject to internalization with rate λ_C, and upon pMHC dissociation, the activated TCR is also marked for internalization (T^*) with rate λ_T, and reverts to the basal state with the rate μ.

The accumulation of TCR in the contact interface is mediated by diffusion, directed transport on the membrane (*2*), and by polarized recycling (*8*). We captured these processes with a single parameter (β) in the equation for T, and for simplicity we assumed this parameter to be constant.

Future work is needed to determine whether the rate of recycling is dependent on the TCR-pMHC reaction rates. We note that these processes may balance the internalization of the TCR and therefore maintain a constant concentration of the TCR at the contact interface, as assumed by our simple productive hit rate model and previously discussed (*8*).

The concentration of free TCR was initially 50 μm^{-2}, the concentration of free pMHC is indicated, and all other species were initially zero. The ODEs were integrated in Matlab (Mathworks) for 4 hours and the numbers of internalized TCRs were recorded. The results from this model are summarized in fig. S1 (row 4). We found that an optimal k_{off} was prominent at a low concentration of pMHC, but became less evident at higher concentrations, as previously reported with a more detailed PDE model (*9*). The dose-response in this case still exhibited differences in E_{max}.

In summary, alternate formulations of the productive hit rate model may exhibit optimal k_{off} rates, but only in limited parameter regimes; however, all formulations of the productive hit rate model predicted differences in E_{max}, whereas the affinity model did not (fig. S1, column 2). We therefore stress that although variants of the productive hit rate model may not exhibit an optimal off-rate, our main conclusions are unchanged. Our finding that measurements of EC_{50} could not be used to discriminate between the affinity and productive hit rate models, whereas E_{max} could, is not dependent on the details of the productive hit rate model. The strength of the present model is that it is simple and can explain several observations. Future experimental work is necessary to refine the productive hit rate model to determine, for example, whether an optimal k_{off} is observed.

Optimized dose-response protocol

Many experimental procedures rely on dose-response assays to obtain estimates of EC_{50} and E_{max}. A common protocol to determine the dose-response curve is to perform repeated measurements at a limited number of concentrations of pMHC. This protocol is illustrated with simulated noisy data in fig. S9A, in which the response is measured four times (gray solid circles) at nine different concentrations of pMHC. Fitting the mean response (black solid circles) with a Hill function provided estimates of EC_{50} and E_{max}. An alternative protocol is to measure the response at 36 different doses with no repeated measurements (fig. S9B), and then fit a Hill function directly to the data. Note that in both protocols, 36 measurements were made.

To determine which protocol provided the most accurate estimates of EC_{50} and E_{max}, we simulated noisy experiments that determined the dose-response curve under each protocol and then compared the estimated EC_{50} and E_{max} values with their true values. At a particular dose (x), we obtained the true response (y) with the following sigmoid function:

$$y = A_1 + \frac{E_{max}}{1 + 10^{n(\log_{10}(EC_{50}) - \log_{10}(x))}} \quad (2)$$

where A_1 is the background response, E_{max} is the maximum response, n is the Hill coefficient, and EC_{50} is the dose at which the response is 50% of the maximum. To simulate dose-response experiments, we added 10% normally distributed noise to the true response (solid gray circles, fig. S9). We next fitted the Hill function to the simulated data directly (gray solid circles,

protocol 2, fig. S9B) or to the mean of four repeated simulated measurements (black solid circles, protocol 1, fig. S9A) to obtain estimates of EC_{50} and E_{max}, which we could then compare to their respective true values.

In the example of fig. S9, the true $\log_{10}(EC_{50})$ was -0.25 and the true E_{max} was 1. For the simulated data shown in this figure, we see that the second protocol provided a better estimate of $\log_{10}(EC_{50})$ (-0.149 as compared to -0.252), but both protocols provided accurate estimates of E_{max} (A_2 =0.977 in protocol 1 and A_2 =0.966 in protocol 2). We formalized this observation by generating 10,000 simulated dose-response curves for each protocol, performing data fitting, and recording the fitted value of EC_{50} and E_{max}. The distributions of the fitted EC_{50} and E_{max} for each protocol are shown in fig. S10. As expected, all distributions are centered on the true values (vertical dotted black line). The relevant quantity is the standard deviation, σ, of these distributions which quantifies the accuracy of the fitted parameter. We found that σ was a factor of 2 smaller for the distribution of EC_{50} when using protocol 2 compared to protocol 1. In other words, protocol 2 provided more reliable estimates of EC_{50}. We found that σ =0.025 for the distribution of E_{max} in both protocols, indicating that both protocols provided equivalent accuracy in determining this parameter.

The second protocol provided a better estimate of EC_{50} compared to the first protocol because it contained more data points along the transition from A_1 to A_2. This is illustrated in fig. S11, in which σ was recorded for the distribution of fitted EC_{50} values as a function of the true EC_{50}. In protocol 1 (fig. S11A), we found that σ depended on the true EC_{50}, achieving large values (and hence poor estimates of EC_{50}) when the true $\log_{10}(EC_{50})$ was ±0.25, and small values when the true $\log_{10}(EC_{50})$ was -0.5, 0, and 0.5. This dependency arose because the concentrations of pMHC were fixed and taken at intervals of 0.5 (see fig. S9A). On the other hand, we found that σ was small and independent of the true EC_{50} in protocol 2 (fig. S11B). This is further emphasized by the observation that if the dose-response curve became less steep (for example, by smaller Hill numbers) then σ decreased. Note that directly fitting the 36 measurements in protocol 1 instead of averaging first produced the same conclusions.

In summary, although both protocols contained 36 measurements, protocol 2 provided more accurate estimates of EC_{50} than did protocol 1. Published studies often follow protocol 1; therefore we expect that the use of protocol 2, as we have done here, will lead to improvements in estimating potency.

Effects of confinement time by TCR/pMHC rebinding

The mathematical models we used in the main text rely on standard mass action, and therefore the model assumes that TCR-pMHC interactions occur in the reaction-limited regime; however, the rate of TCR-pMHC binding at the contact interface is likely to be limited by diffusion (*10–12*). To modify the model described in the main text to include the role of diffusion, we may simply transform the reaction rates to the membrane coupling (k_c) and uncoupling (k_u) rates (*13*):

$$\begin{aligned} k_c &= k_+ k_{\text{on}}/(k_{\text{on}} + k_+) \\ k_u &= 1/T = k_{\text{off}} k_+/(k_+ + k_{\text{on}}) \end{aligned}$$

where k_+ is the diffusion-limited on-rate. In this model, $T = 1/k_u$ is the previously described TCR-pMHC confinement time (*11*). In this way, we can see that the revised predictions from the productive hit rate model (upon the transforms $k_{on} \rightarrow k_c$ and $k_{off} \rightarrow k_u$) are such that EC_{50} remained unchanged, but E_{max} is now predicted to contain a dependency on k_{on} through the uncoupling rate:

$$\begin{aligned} EC_{50} &= K_D + T_T/2 \\ E_{max} &= k_u T_T A f(k_u) t \end{aligned}$$

The functional form of f is unknown, but for simplicity we examined whether a direct linear correlation between E_{max} and k_u could improve the fit beyond the standard mass action model. The data fitting was performed as previously described (*11*). We found no improvement in the fit for the G10 system (fig. S12A), but some improvement in the 1G4 system (fig. S12B). The lack of improvement in the G10 system likely stems from the smaller variability in k_{on} for that system. In the future, it will be important to accumulate data with more pMHCs to determine the precise contribution of k_{on} to maximal antigen efficacy.

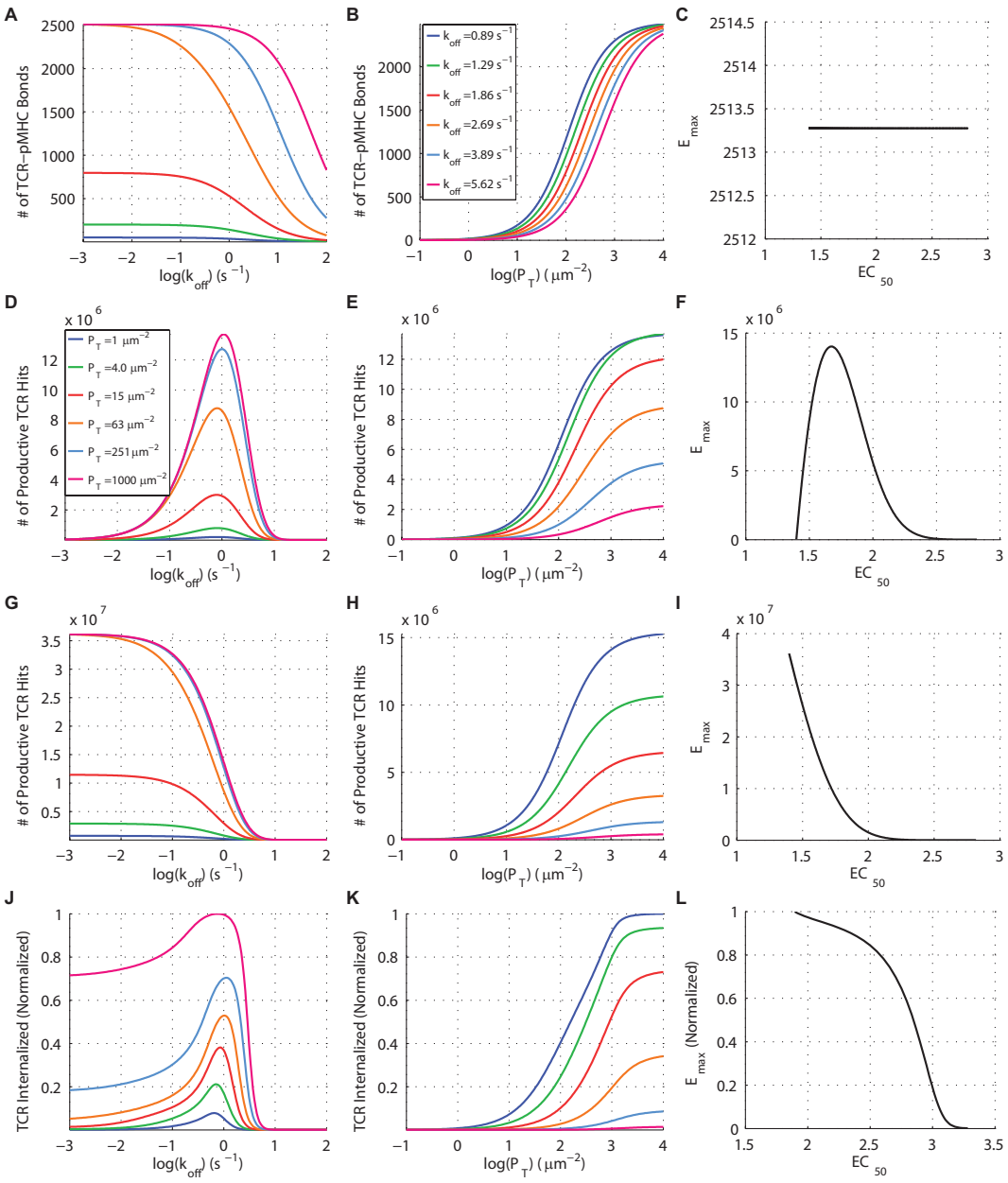

Fig. S1. Comparison of the affinity model with three formulations of the productive hit rate model. The predicted T cell response is shown as a function of k_{off} in column 1, as a function of antigen dose (P_{T}) in column 2, and in column 3, we illustrate the predicted relationship between EC_{50} and E_{max}. The calculations were performed for: (**A** to **C**) the affinity model, (**D** to **F**) the productive hit rate model, (**G** to **I**) the productive hit rate model with continuous TCR signaling, and (**J** to **L**) the productive hit rate model with TCR internalization (see Fig. 2 for details). See the Supplementary Materials for further details.

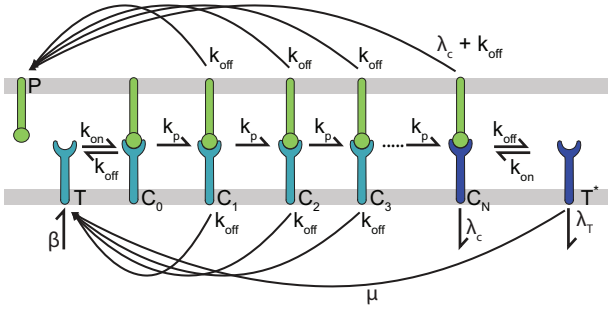

Fig. S2. Productive hit rate model with internalization. The model shown is adapted from Coombs *et al.* (4). In addition to kinetic proofreading, this model incorporates the internalization of TCR upon productive signaling with the rate λ_{C} if the TCR is in complex with pMHC, and with the rate λ_{T} if the TCR is dissociated from the pMHC. TCRs that are marked for internalization but are not bound to pMHC (T^*) revert back to the basal state at the rate μ. The model was initialized with free TCR at a concentration of $T = 50$ μm^{-2}, and with free pMHC at the indicated concentration (P_{T}). The system of ordinary-differential-equations was integrated for 4 hours to determine the number of internalized TCRs. Parameters: $\lambda_{\mathrm{T}} = 0.003$ s^{-1}, $\lambda_{\mathrm{C}} = 0.003$ s^{-1}, $\mu = 0.001$ s^{-1}, $\beta = 0.1$ μm^{-2}/s, $k_p = 1.5$ s^{-1}, and $N = 10$. Parameter estimates are discussed in Coombs *et al.* (4).

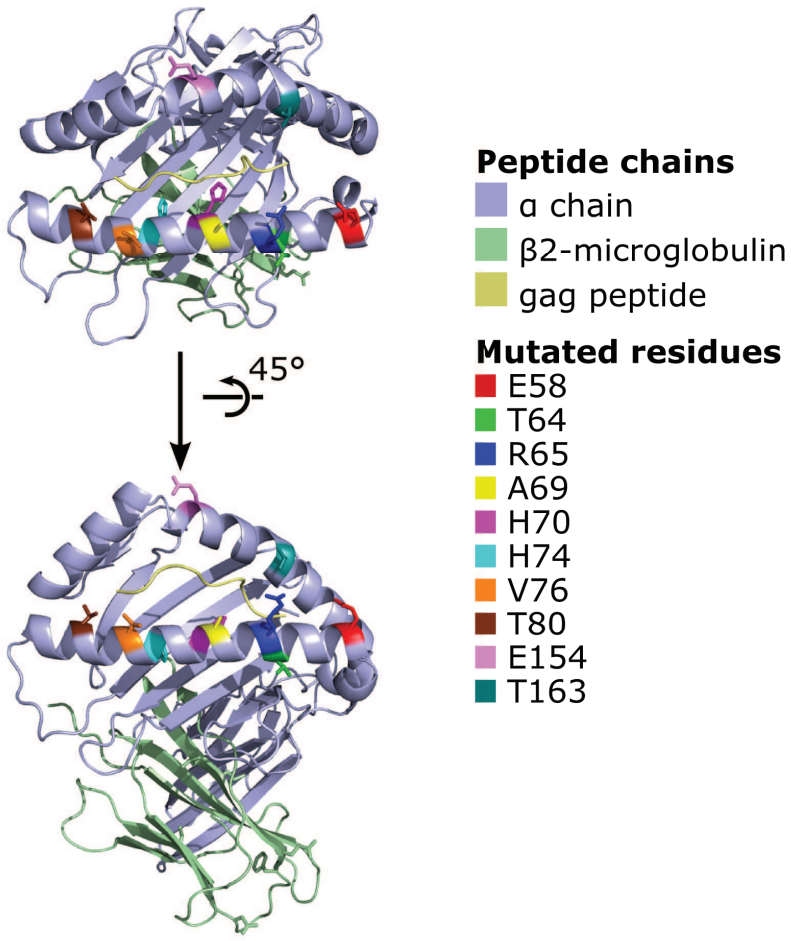

Fig. S3. Structure of the gag peptide in complex with HLA-A2. The gag peptide (SLFNTVATL) is shown in complex with HLA-A2, based on PDB file: 2V2X. The ten mutations sites used in the present study are indicated with their side chains. Mutations sites were chosen to minimize peptide interactions. Using a conformationally sensitive antibody to HLA-A2, we observed very similar pMHC expression across the various mutants (see fig. S4).

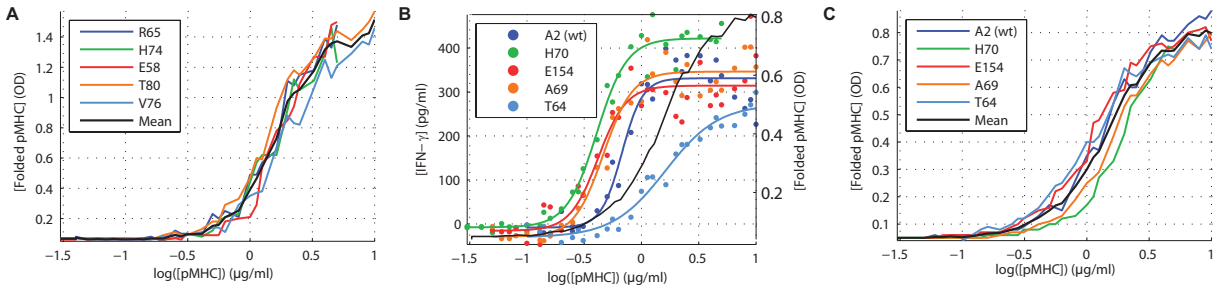

Fig. S4. Complete dose-response data for the G10 TCR system. (**A**) Correctly folded pMHC amounts determined using the W6/32 mouse anti human MHC class I antibody specific for correctly folded pMHC. The black line shows the mean concentration of the five pMHCs that are presented in Fig. 2A. (**B**) Dose-response data for additional pMHCs. As before, the solid black line represents the mean concentration of correctly folded pMHC. (**C**) Concentrations of correctly folded pMHCs for those pMHCs shown in (B). See the Supplementary Materials for additional details.

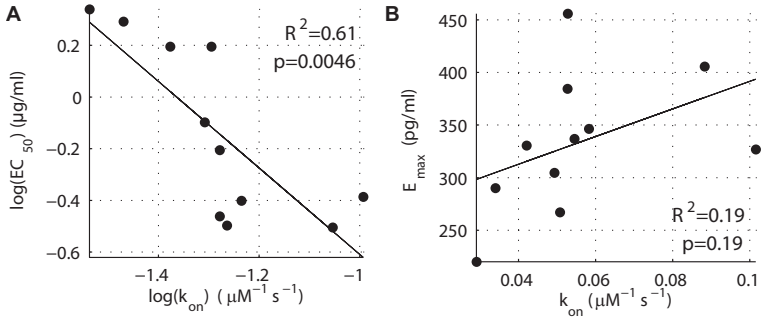

Fig. S5. Additional correlations between reaction parameters and functional response for the G10 CTLs. Correlations between K_{D} and EC_{50} and between k_{off} and $\mathrm{E}_{\mathrm{max}}$ were shown in Fig. 2. Additional correlations are shown between (**A**) k_{off} and EC_{50}, (**B**) K_{D} and $\mathrm{E}_{\mathrm{max}}$, (**C**) k_{on} and EC_{50}, and (**D**) k_{on} and $\mathrm{E}_{\mathrm{max}}$.

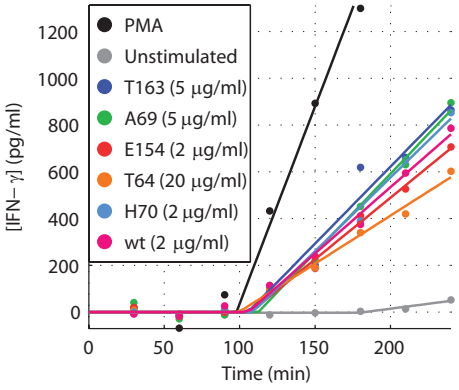

Fig. S6. Time-course data for additional pMHCs. Time-course data are shown for additional pMHCs not shown in Fig. 3A.

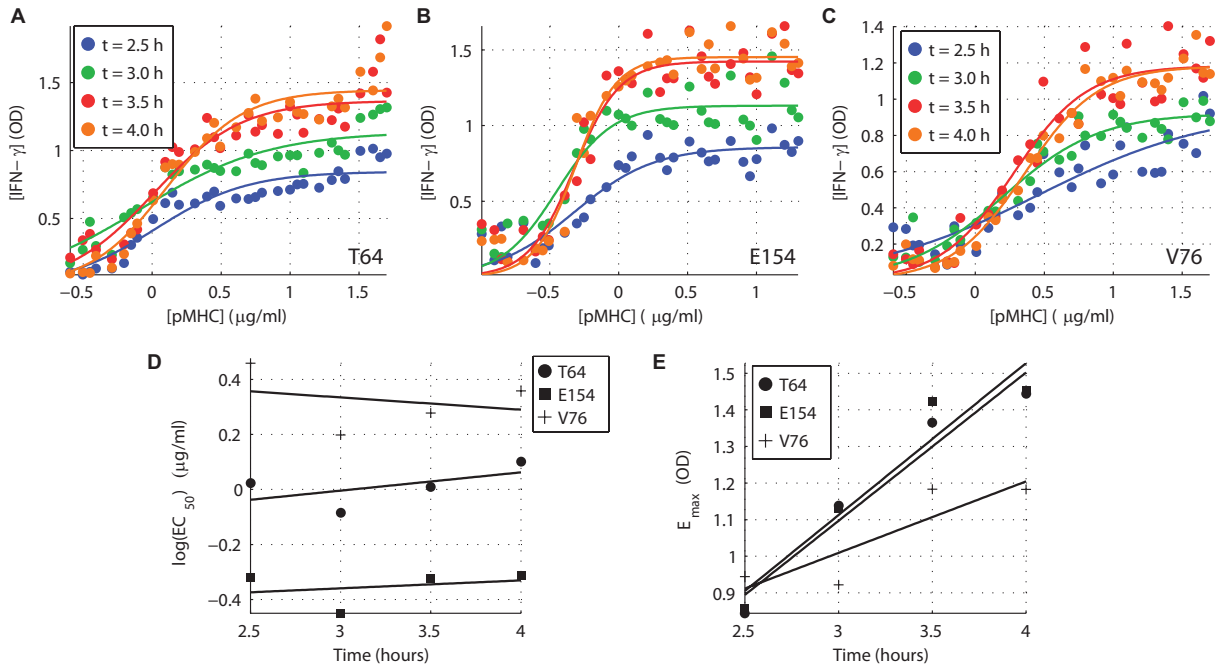

Fig. S7. Confirmation of the time-dependency of E_{max} and the time-independency of EC_{50} . (**A** to **C**) The full dose-response curve was performed for the indicated pMHC at four different time points. The experimental data (solid circles) were fit to a Hill function (solid lines) to estimate the potency and maximal efficacy. (**D** and **E**) As expected, potency was time-independent (D), but maximal efficacy increased with time (E).

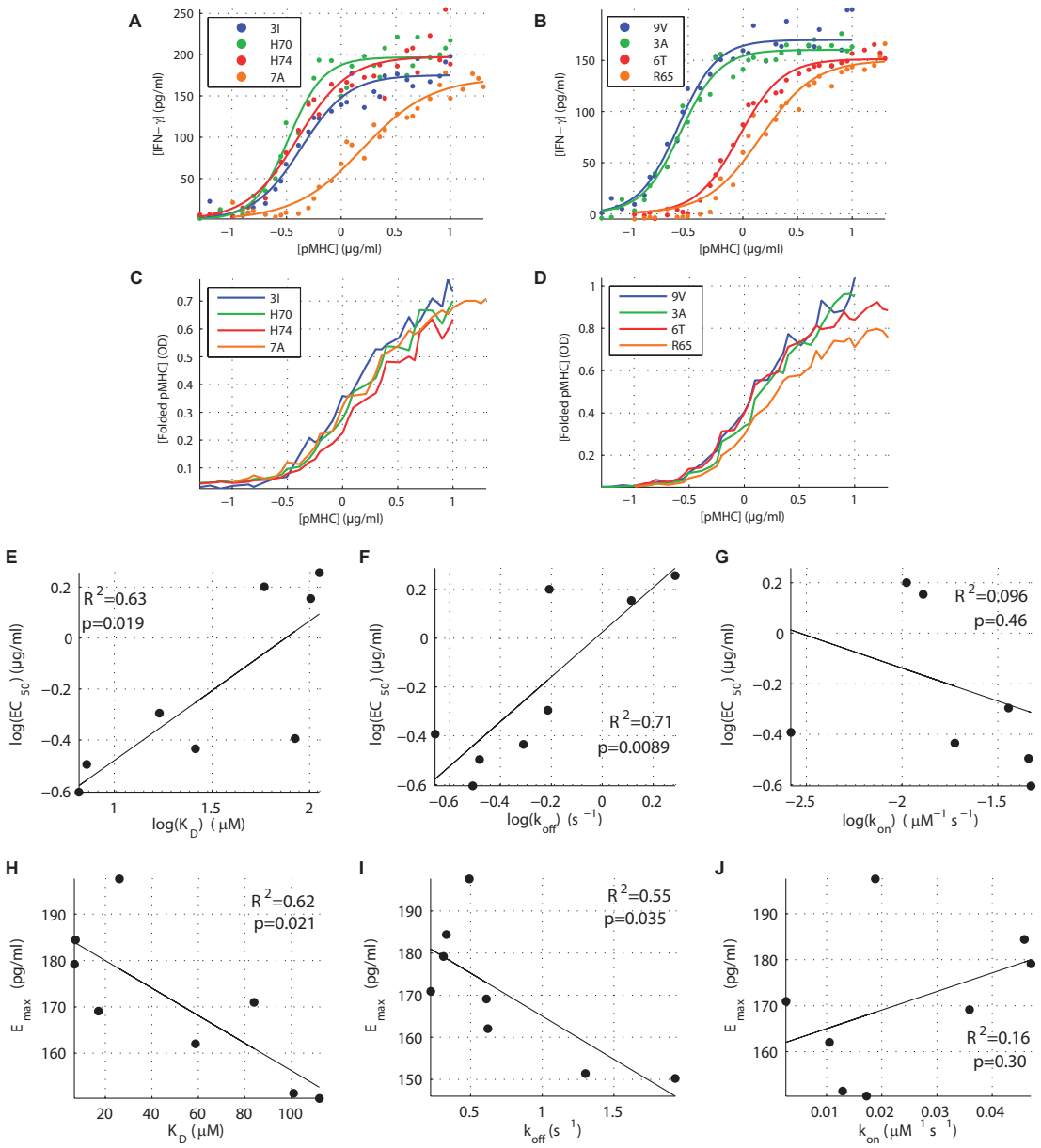

Fig. S8. Confirmation of the relationships between K_{D} and EC_{50} and between k_{off} and $\mathrm{E}_{\mathrm{max}}$. Dose-response assays were performed with the 1G4 CTL clone and 8 pMHC variants. (**A** and **B**) 1G4 CTLs were stimulated as described for the G10 CTLs. (**C** and **D**) Concentrations of correctly folded pMHCs were determined as described for fig. S4. The fitting of a Hill function provided estimates for potency and maximal efficacy. Correlations with (**E** to **G**) antigen potency and (**H** to **J**) maximal efficacy revealed the predicted relationship between (E) K_{D} and EC_{50} and (I) k_{off} and $\mathrm{E}_{\mathrm{max}}$. Note that the latter relationship was determined by the functional form of f(koff); therefore a linear correlation was not necessarily expected. Indeed, the relationship in (I) appears to be nonlinear. All data are summarized in table S2.

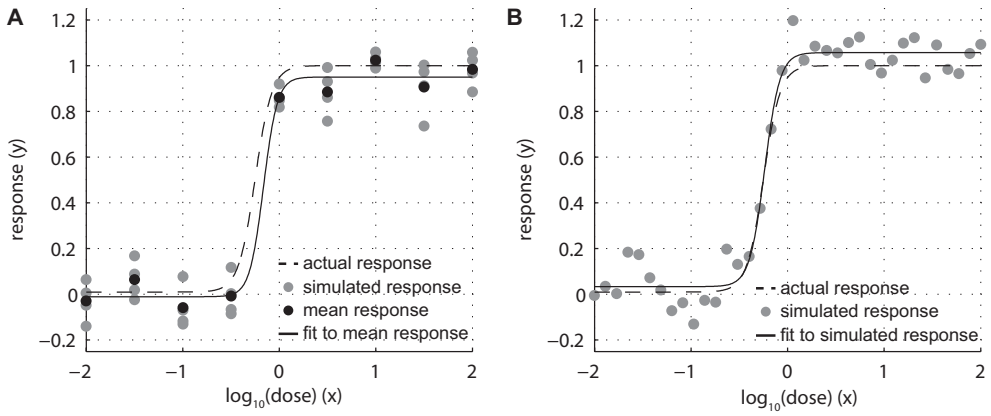

Fig. S9. Simulated dose-response curves using protocols 1 and 2. Simulated dose-response curves using (**A**) protocol 1 (4 measurements at 9 different doses) and (**B**) protocol 2 (1 measurement at 36 different doses) were generated. In both cases, each measurement was obtained by sampling the response (y) from a sigmoid [with true parameter values: $A_1 = 0.01$, $A_2 = 1$, $n = 5$, and $\log_{10}(\mathrm{EC}_{50}) = -0.25$] to which 10% normally distributed noise was added. Individual measurements are shown as gray circles. In protocol 1 (A) the four measurements at each dose were averaged (black circles), and the resulting nine data points were fit to a sigmoid. In protocol 2 (B) the 36 measurements were fit directly to the sigmoid. Sigmoid fits are shown as solid black lines, and the true sigmoid is shown as a dashed black line. Fitted parameters are: $A_1 = -0.011$, $A_2 = 1.06$, $n = 5.2$, and $\log_{10}(\mathrm{EC}_{50}) = -0.12$ for protocol 1 (A); and $A_1 = 0.011$, $A_2 = 0.98$, $n = 4.4$, and $\log_{10}(\mathrm{EC}_{50}) = -0.28$, for protocol 2 (B).

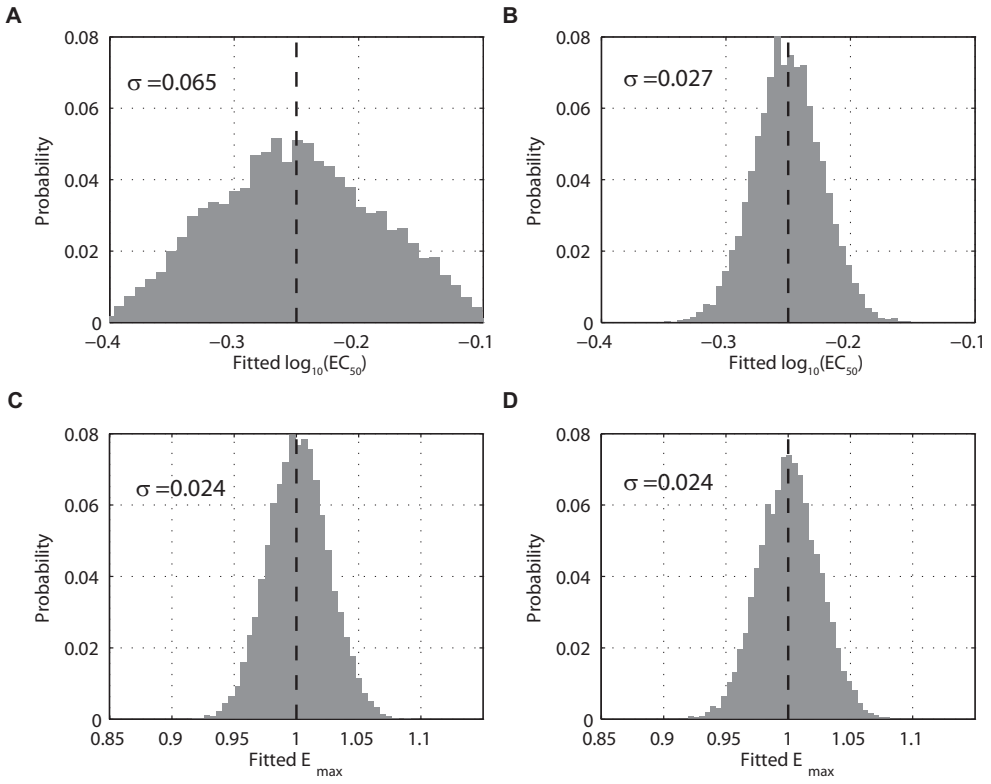

Fig. S10. Histogram of estimated EC_{50} and E_{max} values from protocols 1 and 2. (**A** to **D**) Histograms of estimated EC_{50} and E_{max} with protocol 1 (A and C) and protocol 2 (B and D) are shown. In all cases the distributions are centered on the correct values of EC_{50} and E_{max} (vertical dashed black line). The key features of these distributions are their standard deviations, which partially reflect the noise in the simulated data. However, examining (A) and (B), it can be seen that the distribution of EC_{50} is roughly twice as wide for protocol 1 as for protocol 2 ($\sigma = 0.058$ for protocol 1, whereas $\sigma = 0.031$ for protocol 2). Thus, protocol 2 is more likely than protocol 1 to provide an accurate estimate of EC_{50}. The distribution of E_{max} was similar in both protocols. All true parameter values were as described for fig. S9.

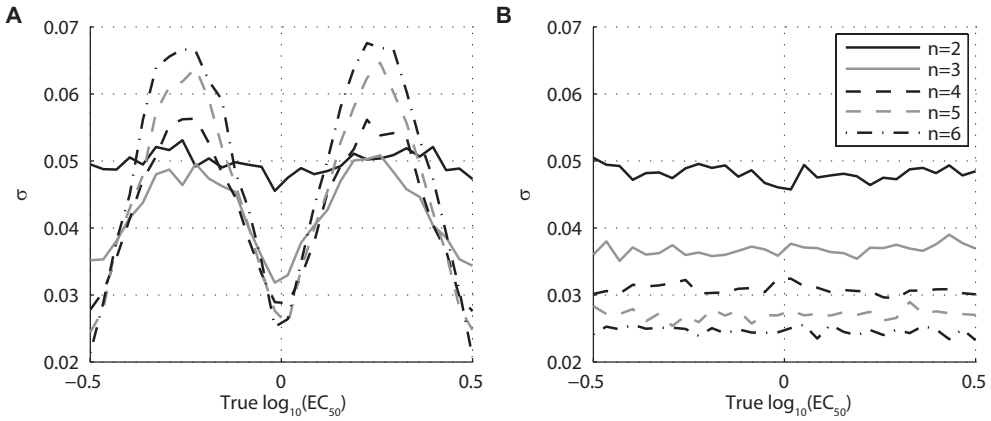

Fig. S11. Standard deviations in the EC_{50} histograms from protocols 1 and 2. The standard deviation (σ) in the distributions of fitted EC_{50} for (**A**) protocol 1 and (**B**) protocol 2 are shown. We recorded σ for each protocol by repeating the procedure outlined in fig. S10 for different values of the true EC_{50} (x-axis). We saw that unless the true EC_{50} coincided with a sampled dose ($10^{-0.5}$, 10^{0}, and $10^{0.5}$), the standard deviation in the distribution of the estimated EC_{50} was large, indicating that protocol 2 (B) provides more accurate estimates than does protocol 1 (A) of EC_{50}. All true parameter values were as described for fig. S9.

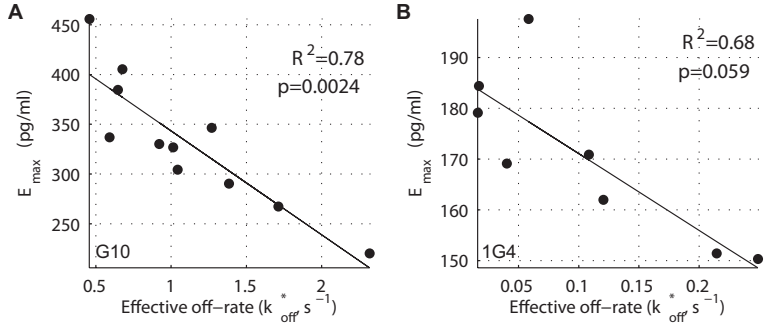

Fig. S12. Effects of TCR-pMHC rebinding in a confinement time model on maximal antigen efficacy. The small diffusion rates of membrane molecules mean that they are likely to rebind before separating by lateral movement through the membrane. Assuming that TCRs continue to signal during brief unbinding events, the relevant membrane off-rate may include a contribution from the on-rate because of rebinding. Fitting for the effective membrane off-rate we find (**A**) no change in the correlation in the G10 system, and (**B**) an improved R^2 for the 1G4 system. The increases in the R^2 and *P* values in (B) compared to the correlation with k_{off} or K_{D} alone (fig. S8, H and I) are because of an increase in the number of fitted parameters for the confinement time model. The few data points for both systems prevented us from drawing definitive conclusions. Future work will be required to examine the effect of rebinding more carefully. Additional details can be found in the Supplementary Materials.

Table S1. Reaction and functional parameters for the G10 TCR.

pMHC		K_D (μM)	k_{off} (s^{-1})	k_{on} ($\mu M^{-1}s^{-1}$)	$\log_{10}(EC_{50})$ (μg/ml)	E_{max} (pg/ml)
R65	SLFNTVATL	9.1± 0.30	0.48± 0.015	0.053± 0.0024	-0.46± 0.12	455.9± 32.6
A2 (wt)	SLFNTVATL	13.0± 0.93	0.68± 0.016	0.053± 0.0040	-0.21± 0.04	384.4± 33.2
H74	SLFNTVATL	8.3± 1.34	0.74± 0.009	0.088± 0.0142	-0.50± 0.10	405.5± 58.6
E58	SLFNTVATL	11.5± 0.66	0.62± 0.012	0.054± 0.0033	-0.50± 0.08	337.0± 74.1
H70	SLFNTVATL	11.0± 1.38	1.12± 0.017	0.102± 0.0128	-0.39± 0.09	326.9± 82.0
T80	SLFNTVATL	35.5± 1.94	1.80± 0.058	0.051± 0.0032	0.19± 0.05	267.2± 53.2
T163	SLFNTVATL	22.9± 0.92	0.96± 0.018	0.042± 0.0019	0.19± 0.02	330.3± 161.2
E154	SLFNTVATL	22.2± 0.40	1.09± 0.014	0.049± 0.0011	-0.10± 0.10	304.5± 64.3
V76	SLFNTVATL	82.2± 5.25	2.38± 0.046	0.029± 0.0019	0.34± 0.08	220.2± 62.1
T64	SLFNTVATL	42.2± 5.23	1.43± 0.047	0.034± 0.0044	0.29± 0.02	290.1± 95.6
A69	SLFNTVATL	23.1± 0.91	1.34± 0.038	0.058± 0.0028	-0.40± ND	346.4± ND

Table S2. Reaction and functional parameters for the 1G4 TCR.

	pMHC	K_D (μM)	k_{off} (s^{-1})	k_{on} ($\mu M^{-1}s^{-1}$)	$\log_{10}(EC_{50})$ (μg/ml)	E_{max} (pg/ml)
9V	SLLMWITQ**V**	7.2± 0.50	0.33± 0.012	0.046± 0.0036	-0.50± 0.01	184.4± 14.3
3A	SL**A**MWITQ**V**	6.6± 0.54	0.31± 0.007	0.047± 0.0040	-0.60± 0.01	179.2± 18.8
3I	SL**I**MWITQ**V**	17.0± 0.88	0.61± 0.039	0.036± 0.0029	-0.30± 0.01	169.1± 6.2
7A	SLLMWI**A**Q**V**	58.7± 3.81	0.62± 0.035	0.011± 0.0009	0.20± 0.05	162.0± 9.9
6T	SLLMW**T**TQ**V**	101.0± 4.61	1.30± 0.033	0.013± 0.0007	0.15± ND	151.4± ND
H70	SLLMWITQ**V**	84.0± 1.65	0.22± 0.006	0.003± 0.0001	-0.39± 0.08	170.9± 25.9
H74	SLLMWITQ**V**	26.0± 0.70	0.49± 0.006	0.019± 0.0006	-0.43± ND	197.6± ND
R65	SLLMWITQ**V**	112.0± 4.94	1.93± 0.126	0.017± 0.0014	0.26± ND	150.3± ND

References

1. C. Wofsy, D. Coombs, B. Goldstein, Calculations show substantial serial engagement of T cell receptors. *Biophys J.* **80**, 606–612 (2001).
2. W. C. Moss, D. J. Irvine, M. M. Davis, M. F. Krummel, Quantifying signaling-induced reorientation of T cell receptors during immunological synapse formation. *Proc. Natl. Acad. Sci. U.S.A.* **99**, 15024–15029 (2002).
3. R. Varma, G. Campi, T. Yokosuka, T. Saito, M. L. Dustin, T cell receptor-proximal signals are sustained in peripheral microclusters and terminated in the central supramolecular activation cluster. *Immunity* **25**, 117–127 (2006).
4. D. Coombs, A. M. Kalergis, S. G. Nathenson,C. Wofsy, B. Goldstein, Activated TCRs remain marked for internalization after dissociation from pMHC. *Nat. Immunol.* **3**, 926–931 (2002).
5. S. Cemerski, J. Das, J. Locasale, P. Arnold, E. Giurisato, M. A. Markiewicz, D. Fremont, P. M. Allen, A. K. Chakraborty, A. S. Shaw, The stimulatory potency of T cell antigens is influenced by the formation of the immunological synapse. *Immunity* **26**, 345–355 (2007).
6. G. Altan-Bonnet, R. N. Germain, Modeling T cell antigen discrimination based on feedback control of digital ERK responses. *PLoS Biol.* **3**, e356 (2005).
7. J. Das, M. Ho, J. Zikherman, C. Govern, M. Yang, A. Weiss, A. K. Chakraborty, J. P. Roose, Digital signaling and hysteresis characterize ras activation in lymphoid cells. *Cell* **136**, 337–351 (2009).
8. S. N. Arkhipov, I. V. Maly, Quantitative analysis of the role of receptor recycling in T cell polarization. *Biophys J.* **91**, 4306–4316 (2006).
9. P. A. Gonzalez, L. J. Carreno, D. Coombs, J. E. Mora, E. Palmieri, B. Goldstein, S. G. Nathenson, A. M. Kalergis, T cell receptor binding kinetics required for t cell activation depend on the density of cognate ligand on the antigen-presenting cell. *Proc. Natl. Acad. Sci. U.S.A.* **102**, 4824–4829 (2005).
10. O. Dushek, R. Das, D. Coombs, A role for rebinding in rapid and reliable T cell responses to antigen. *PLoS Comp. Biol.* **5**, e1000578 (2009).
11. M. Aleksic, O. Dushek, H. Zhang, E. Shenderov, J. L. Chen, V. Cerundolo, D. Coombs, P. A. van der Merwe, Dependence of T cell antigen recognition on T cell receptor-peptide MHC confinement time. *Immunity* **32**, 163–174 (2010).
12. C. C. Govern, M. K. Paczosa, A. K. Chakraborty, E. S. Huseby, Fast on-rates allow short dwell time ligands to activate T cells. *Proc. Natl. Acad. Sci. U.S.A.* **107**, 8724–8729 (2010).
13. D. Shoup, A Szabo, Role of diffusion in ligand binding to macromolecules and cell-bound receptors. *Biophys. J.* **40**, 33–39 (1982).